

1 PassiveVLP: Leveraging Smart Lights for Passive Positioning

2 WEIZHENG WANG, TU Delft, the Netherlands

3 QING WANG, KU Leuven, Belgium

4 JUNWEI ZHANG, TU Delft, the Netherlands

5 MARCO ZUNIGA, TU Delft, the Netherlands

6 Positioning based on visible light is gaining significant attention. But most existing studies rely on a key
7 requirement: the object of interest needs to carry an optical receiver (camera or photodiode). We remove
8 this requirement and investigate the possibility of achieving accurate positioning in a *passive* manner, that
9 is, without requiring objects to carry any optical receiver. To achieve this goal, we propose PassiveVLP in
10 which *we exploit the reflective surfaces of objects* and the unique propagation properties of LED luminaires. We
11 present geometric models, a testbed implementation, and empirical evaluations to showcase the opportunities
12 and challenges posed by this new type of passive positioning. Overall, we show that our PassiveVLP can track
13 with high accuracy (few centimeters) a subset of an object's trajectory and it can also identify passively the
14 object's ID.

15
16 CCS Concepts: • Computer systems organization → Embedded systems; • Networks → Cyber-physical
17 networks;

18 Additional Key Words and Phrases: Visible light positioning (VLP), visible light communication (VLC), passive,
19 reflection of light, system design, implementation, evaluation

20 ACM Reference Format:

21 Weizheng Wang, Qing Wang, Junwei Zhang, and Marco Zuniga. 2019. PassiveVLP: Leveraging Smart Lights
22 for Passive Positioning. *ACM Trans. Internet Things* 1, 1 (July 2019), 25 pages. <https://doi.org/0000001.0000001>

23 1 INTRODUCTION

24 Thanks to advances in the area of Visible Light Communication (VLC), we now have the ability to
25 piggyback wireless communication on top of LED illumination. This technological breakthrough
26 is creating a new range of exciting applications: positioning/localization [Kuo et al. 2014; Li et al.
27 2014; Li and Zhou 2018; Philips 2015; Yang et al. 2017; Zhang et al. 2015; Zhang and Zhang 2017],
28 Internet connectivity via luminaires [802.11.bb 2018; PureLiFi 2012], and a new generation of
29 interactive toys [Corbellini 2014], to name a few. Among these applications, positioning is arguably
30 one of the areas that is benefiting the most. This is due to the fact that visible light waves have
31 propagation properties that are well suited for estimating range: they attenuate in a smooth and
32 rather deterministic manner. For example, when simple trilateration methods are used with radio
33 frequency signals such as WiFi –which are notorious for having severe multipath effects–, the
34 positioning accuracy is between 2 m and 6 m [Mok and Retscher 2007]. But the same trilateration

35 Authors' addresses: Weizheng Wang, TU Delft, Van Mourik Broekmanweg 6, Delft, 2628 XE, the Netherlands, w.wang-14@
36 tudelft.nl; Qing Wang, KU Leuven, Kasteelpark Arenberg 10 - box 2444, Leuven, 3001, Belgium, qing.wang@kuleuven.be;
37 Junwei Zhang, TU Delft, Van Mourik Broekmanweg 6, Delft, 2628 XE, the Netherlands, zhagjunwei@gmail.com; Marco
38 Zuniga, TU Delft, Van Mourik Broekmanweg 6, Delft, 2628 XE, the Netherlands, m.a.zunigazamalloa@tudelft.nl.

39 Permission to make digital or hard copies of all or part of this work for personal or classroom use is granted without fee
40 provided that copies are not made or distributed for profit or commercial advantage and that copies bear this notice and
41 the full citation on the first page. Copyrights for components of this work owned by others than ACM must be honored.
42 Abstracting with credit is permitted. To copy otherwise, or republish, to post on servers or to redistribute to lists, requires
43 prior specific permission and/or a fee. Request permissions from permissions@acm.org.

44 © 2019 Association for Computing Machinery.

45 2577-6207/2019/7-ART \$15.00
46

47 <https://doi.org/0000001.0000001>

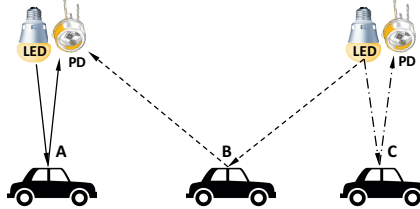


Fig. 1. The concept of passive positioning with smart lights. Three regions *A*, *B*, and *C* can be detected under this simple configuration (PD: photodiode).

methods provide sub-meter accuracy when VLC-enabled luminaires are used as anchor emitting beacons [Li et al. 2014].

Research problem. Current positioning methods based on VLC [Kuo et al. 2014; Li et al. 2014; Li and Zhou 2018; Philips 2015] provide high accuracy but share an important constraint: they require objects to carry photosensors to decode the beacons sent by luminaires. In PassiveVLP, our target is to unleash the constraint of current visible light positioning methods. We remove this constraint and investigate passive visible light positioning, that is, positioning in scenarios where the object of interest does not carry any photosensor. The case we make to investigate *passive* positioning is simple: when objects do not carry photosensors, the only areas that are *constantly* exposed to light are their external surfaces, thus, it's important to *investigate the interaction between VLC luminaires and the reflections coming from these external surfaces to identify cues for positioning*. *Passive* positioning with visible light can be tailored for both static objects and moving objects. The positioning for static objects can exploit the idea from [Li et al. 2015; Xu et al. 2017]. It requires to attach a retro reflector on the surface of the object. Then the system will pinpoint the object according to the light intensities bounced back from the retro reflector to receivers. While, the positioning for moving objects is more appealing to us. Considering this type of scenarios, we want to understand under what conditions would such a positioning system work and what would the expected accuracy be.

Fig. 1 captures the limitations of a naive implementation of passive positioning with visible light. Consider two luminaires that send periodic beacons \mathcal{L}_1 and \mathcal{L}_2 . Each luminaire has a photodiode (PD) attached to it. In general, the PDs co-located with the luminaires may not be able to hear those beacons back due to the low reflectivity of ground surfaces. But if a mobile object with a high reflective surface passes by, the PDs will receive their own (or a neighboring) beacon, and thus, be able to detect the presence of the object. For example, if luminaire \mathcal{L}_1 hears its own beacon, it will infer that an object is in region *A*, and if it hears a beacon from luminaire \mathcal{L}_2 , it will infer that an object is in region *B*. But this basic configuration has three drawbacks: *poor coverage*, few positions can be detected (regions *A*, *B* and *C* in this case); *coarse grained accuracy*, the exact location of the object cannot be determined because we do not know the reflecting angles (shape) of the object; and *there is no identification*, this system can only determine the presence of an object but not its ID, if more than one object is present, the objects cannot be distinguished.

Passive visible light positioning could be applied to scenarios where objects move on established paths in illuminated areas, e.g. mining tunnels or underground train and vehicular systems. In those underground scenarios, radio-based solutions face severe multipath effects, rendering most of those approaches inaccurate.

Our contributions. We propose a novel *passive* positioning system to overcome the above described limitations. Our contributions in this new area are listed below:

- (1) *Geometric model for positioning* (Section 2). We develop a geometric model to identify guidelines for the proper design of the transmitters (luminaires), improve the detection coverage,

99 and increase the positioning accuracy. The model gives us insights on how to design the
 100 transmitters (luminaires) and on what type of objects can be localized with high accuracy.
 101

- 102 (2) *Passive identification* (Section 3). To identify the objects moving under the luminaires, we
 103 embed barcode-like IDs onto the objects' surfaces, and propose a novel framework to decode
 104 these IDs via passive reflections.
 105 (3) *Implementation* (Section 4). We design and implement a testbed to evaluate our system. To
 106 test short-range scenarios, we modify an open platform. For medium-range scenarios, we
 107 develop our own VLC transmitters using standard off-the-shelf LED bulbs.
 108 (4) *Evaluation* (Section 5). We evaluate our system under three different scenarios with increasing
 109 levels of complexity. Our results show that we can pinpoint with cm accuracy a subset of the
 110 object's trajectory and we are able to identify the object's ID in a passive manner.

111 2 MODEL FOR PASSIVE POSITIONING

112 To gain a better understanding about the properties and limitations of passive positioning with
 113 visible light, we use two models: the Lambertian source, which models the radiation pattern of LED
 114 lights; and a geometric model based on the laws of reflection. In the rest of this paper, we focus
 115 on one-dimensional topologies and assume that (i) *LED luminaires are VLC transceivers* (they can
 116 transmit information by modulating their light intensity and they have a photodiode to receive
 117 VLC packets), and (ii) the reflective coefficient of objects is higher than that of the surface where
 118 the object is moving on.

119 2.1 Detecting objects without line-of-sight

120 In VLC, angles play a major role on the received illuminance power. Fig. 2 captures this behaviour.
 121 The wider the irradiation angle ϕ and the wider the incidence angle ψ , the lower the received
 122 illuminance. Also, depending on the LED's optical enclosure, the radiation beam can be long
 123 and narrow, or broad and short. Formally, these relationships are captured by the well known
 124 Lambertian model H . Denoting P_t as the illuminance power of the LED, the received illuminance
 125 power P_r at the photosensor is given by:
 126

$$127 \quad P_r = P_t \cdot H \quad (1)$$

128 where

$$129 \quad H = \begin{cases} \frac{(m+1)A}{2\pi d^2} \cos^m \phi T(\psi) g(\psi) \cos(\psi), & 0 \leq \psi \leq \Psi_c \\ 0, & \psi > \Psi_c \end{cases} \quad (2)$$

130 where m is the lambertian order determining the width and length of the beam, a higher m leads
 131 to a longer and narrower beam; d is the distance between the LED and the photosensor; A is
 132 the detecting area of the photosensor; $T(\psi)$ and $g(\psi)$ are the concentrator and filter gains at the
 133 photosensor; and Ψ_c is the field-of-view of the receiver.

134 The Lambertian model is the pathloss model tailored for line-of-sight communication. It is similar
 135 to the Friis pathloss model for radio. Passive positioning relies on reflected beams (no-line-of-sight).
 136 To capture the effect of reflections, we modify the above equation based on two properties of the
 137 reflective surface; its area A_s and its reflective coefficient ρ .

$$138 \quad H_{NLOS} = H f(A_s) \rho \quad (3)$$

139 where $f(A_s)$ is a linear function of A_s , as explained later. To capture the effect of these two new
 140 parameters, we perform the following experiment. First, we set a transmitter and a receiver at a
 141 two-meter distance with line-of-sight, as shown in Fig. 3, points A and B. Then we put a reflective
 142 surface at point I, one meter away from the LED, and move the receiver to point C (mirror image of
 143 point B).

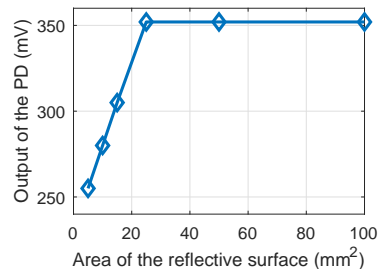
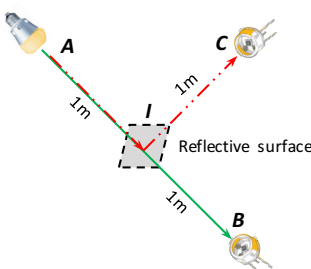
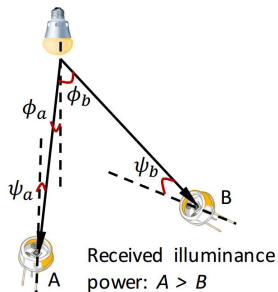


Fig. 2. The Lambertian model. Fig. 3. Capture of reflection effect. Fig. 4. Impact of the area of the reflective surface (used material is mirror).

Table 1. Measured combined coefficient ρ of different materials

Material	Mirror	Aluminum	White cardboard
Coefficient ρ	0.89	0.62	0.30

point B). In this experiment we change the area (A_s) and the material (ρ) of the reflective surface. Our results lead to a design guideline for passive positioning.

Guideline 1: Objects with specular reflection and high reflective coefficients are suitable for accurate positioning. Passive positioning with VLC relies on receivers being able to detect reflected messages. The stronger the reflection, the higher the likelihood of detecting an object (better coverage). Upon impinging an object, a reflected light beam loses intensity in two ways: by the way the beam is reflected (shininess), and by how much light is absorbed by the object (reflection). We combine these two effects into a single parameter ρ . Table 1 shows the coefficients we obtained for three different materials. For the particular setup in Fig. 3, only two materials, mirror and aluminum, would be localizable in our system because their reflection coefficients are high enough to allow the decoding of information after reflection.

Guideline 2: The reflective surface of the moving object A_s should be at least the same size as the receiver's area A . Fig. 4 depicts the effect of changing the area of the reflective surface. For these experiments we use mirrors as the reflecting surface. When the area is small, the received illuminance power is low. Beyond a point however further increasing the area of the reflective surface does not increase the received illuminance power. This occurs because, with specular reflections, the majority of reflections caused by larger areas do not reach the receiver. Thus, a reflective surface that is smaller than the photosensor's surface affects coverage, because it reduces the likelihood of detecting the object.

2.2 Achieving full coverage

The previous subsection indicates that an object only requires a small reflective area to be localized. But this approach only provides limited coverage. In the simplest case, considering N luminaires we would only be able to identify $2N - 1$ points. The N points under the luminaires and the $N - 1$ intermediate points. However, since the size of the reflective surface can be small, an object can carry an array consisting of many small reflecting surfaces but tilted at different angles. The different angles will reflect beams towards the receiver at different locations, improving coverage. Based on simple geometry, we can make the following propositions based on Fig. 5.

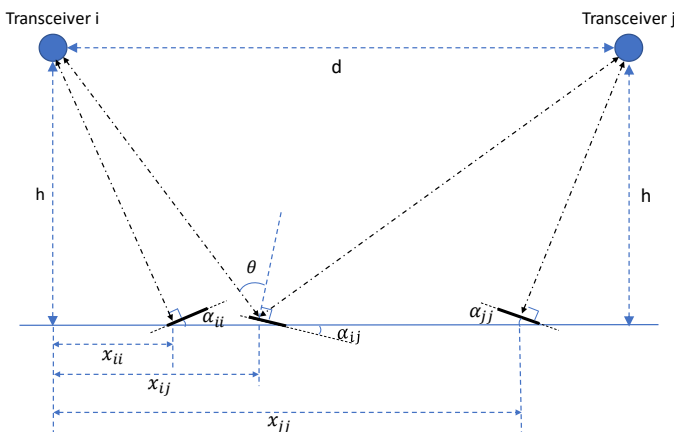


Fig. 5. The illustration of the existences of α_{ij} (Proposition 2.1) as well as α_{ii} and α_{jj} (Proposition 2.2)

PROPOSITION 2.1. Given two neighboring luminaires i and j , with an inter-distance d and height h from the ground; for any given position x between the lights, there is a tilted angle that will reflect light towards a neighboring transceiver:

$$\alpha_{ij} = \frac{\arctan\left(\frac{d-x}{h}\right) - \arctan\left(\frac{x}{h}\right)}{2}$$

where clockwise turns denote positive direction of angles.

PROOF. We leverage Fig. 5 to help visualize the proof. Letting θ be the incidence angle of light on the object, α_{ij} is given by:

$$\alpha_{ij} = \arctan\left(\frac{d-x}{h}\right) - \theta$$

and we can see that

$$\theta = \frac{\arctan\left(\frac{d-x}{h}\right) + \arctan\left(\frac{x}{h}\right)}{2}$$

Hence,

$$\alpha_{ij} = \frac{\arctan\left(\frac{d-x}{h}\right) - \arctan\left(\frac{x}{h}\right)}{2}$$

□

Based on Proposition 2.1, we can get:

PROPOSITION 2.2. For a given position x , there always exists a tilted angle that can make the object reflect light back towards the same transceiver:

$$\alpha_{ii} = -\arctan\left(\frac{x}{h}\right), \quad \alpha_{jj} = \arctan\left(\frac{d-x}{h}\right) \quad (4)$$

PROOF. We leverage Fig. 5 to help visualize the proof. For α_{ii} and α_{jj} , the incidence angle of the light on the object is 0. α_{ii} and α_{jj} are equal to the irradiation angle of the light, which is $\arctan\left(\frac{x}{h}\right)$ or $\arctan\left(\frac{d-x}{h}\right)$. Considering the positive direction of angles, we get that

$$\alpha_{ii} = -\arctan\left(\frac{x}{h}\right)$$

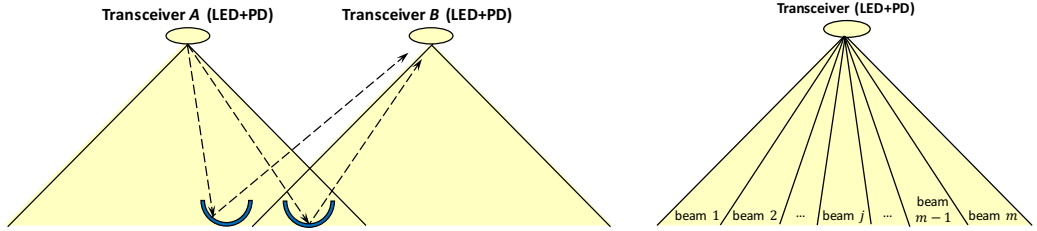


Fig. 6. The problem of unique signature when each transceiver has a single beam (*the object has many tiny reflective surfaces tilted at different angles (kind of ‘retro-reflector’) to improve the coverage)*

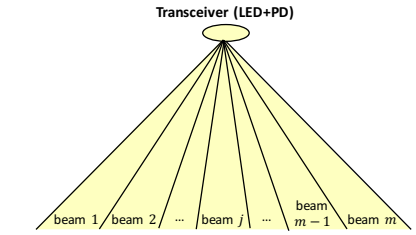


Fig. 7. A transmitter with m beams (*here we use a triangle instead of the Lambertian shape to represent the coverage of an LED, for simplicity.*)

and

$$\alpha_{jj} = \arctan\left(\frac{d - x}{h}\right)$$

□

Guideline 3: *A small polyhedral-reflector can be added on top of the object to provide constant coverage.* Consider an object with a reflective coefficient that is too low to reflect a VLC message. Such an object could not be localized in our system. To solve this problem, we can add polyhedral-reflectors to provide better coverage. A polyhedral-reflector can be created to reflect a wide incoming beam (cm^2) into many outgoing narrow beams (mm^2) in different directions. Note that even if an object has a high reflective coefficient, a polyhedral-reflector can be still used to increase coverage, since few objects have surfaces with multiple tilted angles.

2.3 Obtaining unique signatures

Until now, our guidelines have focused on the issue of coverage (i.e. increase the number of detected points). But we have not tackled the issue of obtaining a unique fingerprint for each detected point. To highlight this problem, let us use Fig. 6. Independently of the location of the object, a neighboring light will always receive the *same* ID, and thus, it would not possible to identify the location of an object. For example in Fig. 6, Luminaire B receives the *same* beacon for the two positions of the convex surface, and thus, it cannot pinpoint the exact location. One way to discern two locations with the same beacon-ID is to use the RSS. But due to the intricate relation among the irradiation and incident angles, the lambertian order m and the distance traveled d ; we observed three problems. First, except for a few points, most RSS values map to multiple locations. Second, the sensitivity of simple photodiodes is not sufficient to distinguish small changes in RSS. Third, under some lighting conditions, the photodiodes can receive the beacons reflected by the ground, which affects the RSS.

Due to the limitations of RSS, we propose to use luminaires with multiple beams, as shown in Fig. 7. Instead of having a single *wide* beam with a low lambertian order, we propose to use multiple *narrow* beams with higher lambertian order. Notice that the overall power does not need to increase, since each narrow beam requires less energy to attain the same range as a wide beam. In our system, each beam emits a unique ID tuple $\langle \mathcal{L}, \mathcal{B} \rangle$, where \mathcal{L} denotes the ID of the luminaire and \mathcal{B} the ID of the beam within that luminaire.

Guideline 4: *Luminaires should be designed with multiple beams, the more beams the better.* It is important to highlight that standard off-the-shelf LED lights already consist of multiple internal LED substrates. Many of these LED substrates point to different directions. Designing VLC luminaires

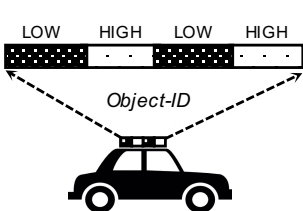


Fig. 8. Attach barcode-like ID to the object's surface

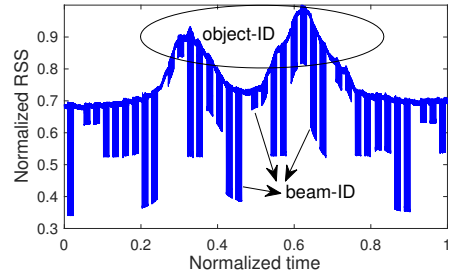


Fig. 9. Illustration of the overlapped signal

for passive positioning would entail adjusting the angles of some of these beams and providing each beam with a unique ID \mathcal{B} .

2.4 Positioning algorithm

Assuming a set of luminaires and objects following our guidelines, the positioning algorithm works as follows.

Step 1: The algorithm requires as inputs: the inter-node distance d , the height of luminaires h , the FoV of the photosensor ω , the number of beams at each luminaire b , a vector μ with the directional angles of the beams, and a vector containing the k tilted angles of the reflector (surface) $\{\alpha_1, \dots, \alpha_k\}$.

Step 2: Using Proposition 1, the transceiver calculates the locations \hat{x}_i for all the tilted angles $\alpha_i, i = 1, \dots, k$. At this point we have k possible locations for the moving object.

Step 3: Upon receiving a beacon from a neighboring light, or from itself, the algorithm computes the region covered by that beam: $[x_{\mathcal{L}, \mathcal{B}}^1, x_{\mathcal{L}, \mathcal{B}}^2] = [h \tan(\mu_{\mathcal{L}, \mathcal{B}} - \omega/2), h \tan(\mu_{\mathcal{L}, \mathcal{B}} + \omega/2)]$. At this point we know the object is under the coverage of beam $< \mathcal{L}, \mathcal{B} >$, but we do not know exactly where.

Step 4: The only valid locations \hat{x}_i (Step 2) are those that fall in the range $[x_{\mathcal{L}, \mathcal{B}}^1, x_{\mathcal{L}, \mathcal{B}}^2]$ (Step 3). If only one estimation \hat{x}_i falls in this range, \hat{x}_i is given as the object's location. If multiple estimations fall in the range, the algorithm either returns the average as the location, or chooses one of the estimations with higher probability if the direction and velocity of the target can be estimated with prior points.

3 PASSIVE IDENTIFICATION

Positioning an object is not enough. We now introduce how to further *identify* the object *passively* in our system.

Our approach is inspired by a recent work that leverages ambient light for passive communication [Wang et al. 2016], which adopts the patterns of distinctive reflecting surfaces to modulate ambient light. In this paper, we use a similar method to label objects with unique IDs attached to objects' surface, as illustrated in Fig. 8. We refer to this 'barcode' as *object-ID*. We use materials with different reflection coefficients to build an object-ID, e.g, aluminium (high) and black paper (low). To decode an object-ID at the PD according to the light it reflects, we have to tackle two challenges:

- *Overlapping signals containing the beam-ID and object-ID.* As presented in Sec. 2, each transmitter sends modulated light containing its *beam-ID*. At certain positions, this modulated light can be *reflected* by the object's surface to the PD and be used to localize the object.

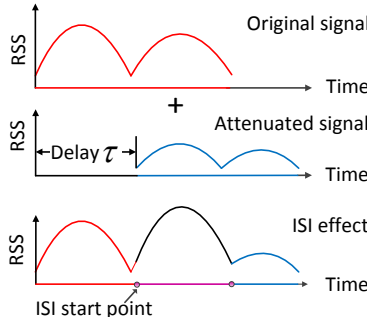


Fig. 10. Illustration of the inter-symbol interference

But the *object-ID* also *modulates* the impinging light, albeit at a lower frequency. Thus, the PD will receive an overlapping signal containing both the beam-ID and the object-ID, as illustrated in Fig. 9. To identify the object, we need to extract the signal that only contains the object-ID from the overlapping signal.

- *Inter-Symbol Interference (ISI)*. At some positions, different parts of the object-ID can reflect concurrently the light coming from two neighbouring beams. Therefore, the light modulated by the object-ID may contain interference caused by itself, namely, an ISI effect. As illustrated later in Fig. 13 of Section 3.2, the lights of beam-1 and beam-2 are modulated by the third symbol (at point A) and the first symbol (at point B) of the object-ID, respectively. This generates ISI at the PD, as shown in Fig. 10. Assuming that the object traverses point A first, then the signal modulated at point B is *actually an attenuated and delayed* version of the original modulated signal at point A. In the rest of this paper, we refer to these two types of signals as *attenuated signal* and *original signal*, respectively.

3.1 Decoupling of overlapping signals

We tackle this problem by proposing a downsampling-based method motivated by the following observations: (i) The signal containing the beam-ID is a *high-frequency signal* (created by modulating LEDs at high speed) while the signal containing the object-ID is a *low-frequency signal* (created by the object's movement); (ii) When the LED transmits OFF symbols (namely, LED is off), there is a drop in the signal intensity received at the PD, as shown in Fig. 9. However, when transmitting ON symbols (namely, LED is on), no drop exists. *In other words, the overlapping signal only occurs when OFF symbols are transmitted. Thus, we just need to remove the OFF symbols from the overlapped signals.* The proposed downsampling method works as follows:

- (1) Guarantee that there are no continuous OFF symbols in the modulated data at the LEDs. This is a necessary requirement to remove the OFF symbols in our method. To achieve this, we use the following modulation at transceivers: use a symbol sequence of OFF-ON to denote a bit 0, and symbol sequence of OFF-ON-ON to denote a bit 1. This modulation is depicted in Fig. 11(a);
- (2) Set the downsampling interval slightly wider than the duration of an OFF symbol. By doing this, we guarantee that each OFF symbol is sampled at most once, as depicted in Fig. 11(b);
- (3) Compare each two adjacent samples: if the difference of two adjacent samples is higher than a threshold (i.e., an abrupt drop occurs in the RSS), then we discard the sample that has a lower value (i.e., remove the OFF symbol).

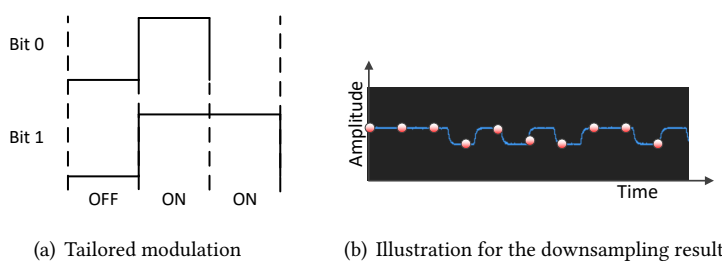


Fig. 11. Proposed downsampling method to decouple overlapping signals

3.2 Remove the inter-symbol interference

As we know, smart lighting has become an effective way to reduce the high energy footprint on artificial lighting. Smart lighting systems adjust the illuminance of artificial lights (normally, LED lights) based on the contribution of ambient natural sunlight in our environment. They are expected to maintain a constant illumination within the area of interest, improving the energy-saving and user-comfort [Wu et al. 2017]. Taking this practical requirement into consideration, the ISI problem described at the beginning of Section 3, can be addressed by different methods according to the requirement on artificial illumination from LEDs. In this paper, operation modes of the LEDs are divided into two types:

- *Communication mode*. When the ambient light is enough to provide illumination, there will be no demand on artificial LED illumination. Therefore, an LED only needs to be turned on when it is scheduled to send its beacon; otherwise, the LED is turned off. This is depicted in Fig. 12(a). When only one LED is turned on at a given time slot, there would not have multiple LED light adding together to form the ISI effect. Therefore, the ISI problem is avoided.
- *Communication+illumination mode*. This mode is enabled when the ambient light is weak. Under this mode, multiple LEDs should be turned on to satisfy the required illumination level. Among these LEDs, one of them is scheduled to transmit its beacon at a given time slot, while the other LEDs are simply turned on to illuminate the surrounding environment, as depicted in Fig. 12(b). As we presented at the beginning of Section 3, this is the main reason why we have multiple signals overlapped with each other that brings the ISI effect.

Under the *communication mode* of LEDs, the ISI problem can be avoided easily. However, in reality the *communication+illumination mode* of LEDs is more common and also more challenging. Therefore, in the rest of this subsection, we will present our general solution to remove the ISI effect considering the *communication+illumination mode* of LEDs.

To eliminate the ISI effect, we propose a method to remove the attenuated signal from the original one. To do this, we need the following information: (1) *delay* of the attenuated signal with respect to the original signal; and (2) *intensity* of the attenuated signal. Next we present how to obtain these information and how to extract and decode the original signal after that.

- **Obtaining the delay of the attenuated signal** Consider the scenario in Fig. 13. As presented earlier in this section, the ISI starts when the object reaches point B. At this position, a symbol (e.g., the i th symbol) of the object-ID will generate interference by modulating the light emitted by beam-2. Note that this modulated light contains the ID of beam-2 and this beam-ID can be decoded by the PD for localization. Moreover, when reaching point A, this i th

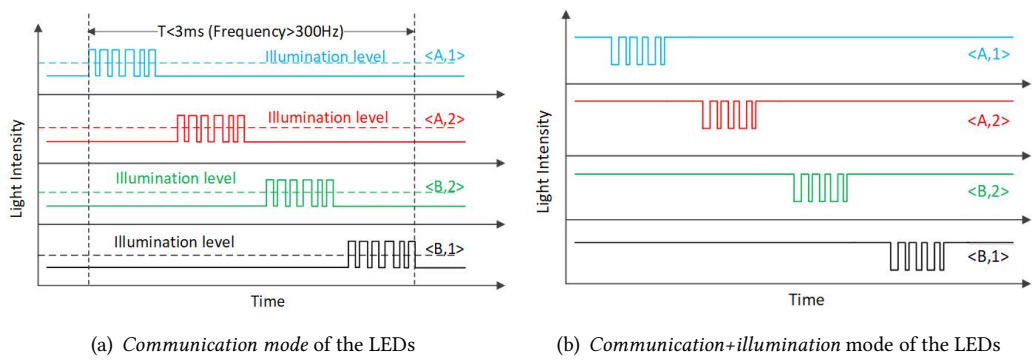


Fig. 12. Operation modes of the LEDs under different ambient light conditions

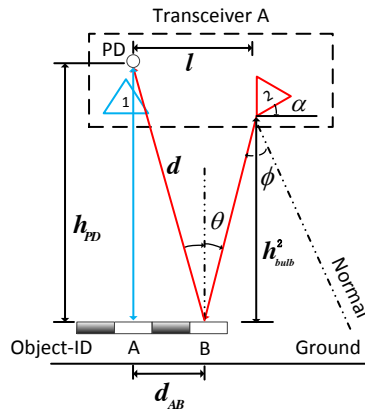


Fig. 13. Illustration of the geometric model used to remove the ISI

symbol has modulated the light emitted by beam-1, and this modulated light carrying the ID of beam-1 has been decoded by the PD as well.

Let t_0 and $t_0 + \tau$ be the time when *for the first time* the PD decodes the IDs of beam-1 and beam-2, respectively. Since the transceiver can modulate light at a very high speed (i.e., it can transmit the frames that contain beam-IDs very frequently), we can assume that t_0 and $t_0 + \tau$ are the time when the object reaches point A and point B, respectively.

Therefore, the difference between t_0 and $t_0 + \tau$, namely, τ , is the delay of the attenuated signal. Note that t_0 and $t_0 + \tau$ can be obtained easily in practice. Besides, at some positions (as will be presented in Sec. 5.3), τ can be a negative value, meaning that the attenuated signal starts earlier than the original signal.

- **Obtaining the intensity of the attenuated signal** To derive this, we still use Fig. 13 as an illustration. Let h_{PD} and h^2_{bulb} denote the heights of the PD and bulb 2, respectively, and let l be the horizontal distance between them. From the geometric model in Fig. 13, we can derive the distance d_{AB}

$$d_{AB} = l \cdot \frac{h_{PD}}{h_{PD} + h^2_{bulb}} \quad (5)$$

Let θ and ϕ be the reflection angle at point B and irradiance angle of bulb 2, respectively. We have $\theta = \arctan \frac{d_{AB}}{h_{PD}}$ and $\phi = \alpha + \theta$. Based on Eq. (1), we can obtain the intensity of the attenuated signal modulated by the object-ID at point B :

$$P_{\text{att}}^B = \frac{\rho P_t (m+1) \cos^m(\phi)}{2\pi d^4} T(\theta) g(\theta) \cos(\theta) \quad (6)$$

Similarly, the intensity of the original signal modulated by the object-ID at point A can be expressed as follows:

$$P_{\text{orig}}^A = \frac{\rho P_t (m+1) \cos^m(0)}{2\pi h_{PD}^4} T(0) g(0) \cos(0) \quad (7)$$

In our model, we can assume that $h_{PD} \approx h_{\text{bulb}}^2 \gg l$. Then we have the approximation: $h_{PD} \approx d$. Besides, there is no optical filter or concentrator in our system. Thus, $T(\cdot)$ and $g(\cdot)$ are constant in our model. Let η denote the *attenuation ratio*, defined as the ratio between the intensity of the attenuated signal and that of the original signal, then we have

$$\eta = \frac{P_{\text{att}}^B}{P_{\text{orig}}^A} = \cos^m(\phi) \cos(\theta) \quad (8)$$

- **Extract and decode the original signal** To achieve this, from now on we consider the continuous version of the signals. Following convention, we use $f(t)$ to denote a continuous signal. Let $f_{\text{orig}}(t)$ and $f_{\text{att}}(t)$ be the continuous original signal and the continuous attenuated signal, respectively. We have

$$f_{\text{att}}(t) = \eta f_{\text{orig}}(t - \tau) \quad (9)$$

Let $f_{\text{sum}}(t)$ be the aggregated signal received at the PD, then

$$f_{\text{orig}}(t) = f_{\text{sum}}(t) - f_{\text{att}}(t) = f_{\text{sum}}(t) - \eta f_{\text{orig}}(t - \tau) \quad (10)$$

As presented in Sec. 3.2, we can denote t_0 as the time when the object-ID reaches point A and $t_0 + \tau$ as the time when the object-ID reaches point B where the ISI appears. Since there is no ISI during the time slot $[t_0, t_0 + \tau]$, we have

$$f_{\text{orig}}(t) = f_{\text{sum}}(t), \quad \forall t \in [t_0, t_0 + \tau] \quad (11)$$

Based on Eq. (10) and Eq. (11), we can now obtain the original signal $f_{\text{orig}}(t)$ (without the ISI effect). To decode it, we use a simple threshold-based decoding method (omitted due to its simplicity, limited novelty, and the page limitation).

3.3 Object-ID design

As mentioned at the beginning of Section 3, we use materials with different reflection coefficients to build an object-ID, e.g, aluminium (of high reflection) and black paper (of low reflection). An object-ID consists of two parts: *object-ID-preamble* and *object-ID-value*. In these two parts, we use materials with both high reflection coefficient (referred as ‘HIGH’ in the rest of this paper) and low reflection coefficient (referred as ‘LOW’ in the rest of this paper) to embed the information. The structure of our designed object-ID is given in Fig. 14. The PD’s captured signal of the designed object-ID is illustrated in Fig. 15. The *object-ID-preamble* plays an important role on decoding the object-ID at the PD. Therefore, we first present our key considerations when designing the preamble.

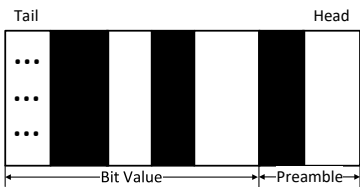


Fig. 14. The structure of our object-ID

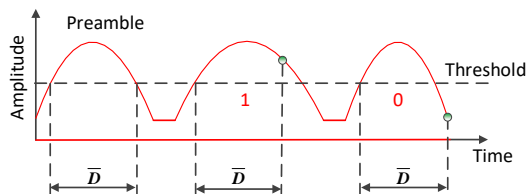


Fig. 15. Illustration of the PD's captured object-ID signal

3.3.1 Object-ID-preamble design. The preamble can be used to obtain the threshold which is key to decode the following ID part of the object-ID. Besides, it can help estimate the speed of objects. Remember that we have ISI effect when multiple LEDs operate at the *communication+illumination* mode. Although we can remove the ISI effect with the mechanism introduced in Section 3.2, it is better if we can design an *ISI-free object-ID-preamble*. Denoting the length of object-ID-preamble as L_p . An improper L_p will bring ISI effect as well as making it difficult to locate the right ISI starting point in the signal. For instance, as illustrated in Fig. 16, if L_p is longer than d_{AB} (cf. Fig. 13), then the ISI effect occurs and it is not easy to calculate the ISI starting point, which is crucial for the mechanism we propose in Section 3.2.

To avoid the above problem, we design the object-ID-preamble length L_p to be equal to or smaller than d_{AB} . This means that, as illustrated in Fig. 16, the attenuated signal starts from the second valley in the original signal (when $L_p = d_{AB}$), or after the second valley (when $L_p < d_{AB}$). In this work, we set $L_p = d_{AB}$. By doing this, we not only achieve an ISI-free preamble for the object-ID, but also know that the ISI starts from the second valley of the original signal. Note that when L_p is too short, it is not easy for the PD to detect the preamble. In passiveVLP, the appearance duration of the Object-ID-preamble at the PD should be much longer than the time needed to transmit a beacon, in order for the PD to decode correctly the beacons. This can be seen clearly from Fig. 9, where the duration of object-ID is much longer than that of an beam-ID.

In the preamble, we use one HIGH and one LOW, starting from HIGH, i.e. the preamble has the pattern of HIGH-LOW. The total length of the HIGH and the LOW in the preamble equals to L_p . This design of the preamble is shown in Fig. 17. In reality, it is possible that the distance between the object-ID and the ceiling PD varies (e.g. the ceiling is not flat in the underground scenario). Therefore, L_p could not always be the same as d_{AB} . In this case, the second valley in the combining signal will no longer be the ISI starting point. Therefore, we need to find the minimum length of LOW to make the second valley as long as possible, to form a flat area. Then, the beginning of the rising trend will become the ISI starting point.

3.3.2 Object-ID-value design. Following the used pattern in the preamble, in the object-ID-value part, we also use the pattern HIGH-LOW to denote each bit of the object ID. For example, if there are four bits to denote the value of the object ID, then we will have four groups of HIGH-LOW in the object-ID-value part. To distinguish between a bit 1 and a bit 0, we use different durations for the HIGH and LOW in the corresponding group of HIGH-LOW, as illustrated in Fig. 17.

4 TESTBED

A solid evaluation of passive positioning with VLC requires designing a system where multiple parameters can be adjusted. Below we describe how we use our design guidelines to build a comprehensive evaluation testbed.

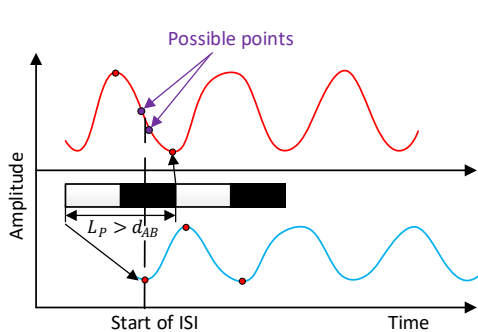


Fig. 16. Illustration of the starting point of the ISI effect



Fig. 17. Bit design in PassiveVLP

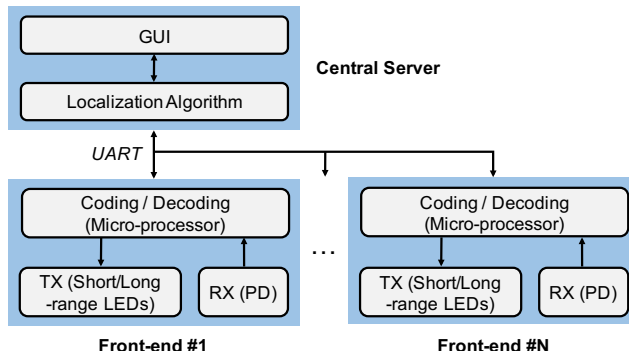


Fig. 18. The function blocks of our PassiveVLP testbed

4.1 Luminaire design

We design our luminaires based on the Shine platform [Klaver and Zuniga 2015]. Shine was originally designed for omni-directional multi-hop communication with visible light. Each Shine node is equipped with 20 LEDs (HLMP-CM1A-450DD, FoV is 18°); and four PDs (SFH203P, FoV is 90°). The micro-controller is an Atmega 328P, which is low-cost but powerful. Shine also provides serial communication capability to interface with a PC/laptop. We extend it largely in both the hardware and software to build our testbed in three ways. First, we improve its reception capabilities, a front-end we refer to as *Shine+*. Second, we add more powerful LEDs to build another front-end referred as *Shine++*. Third, we modify its software. The block diagram of our new testbed is given in Fig. 18. Next, we present the design details of both front-ends.

4.1.1 A short-range luminaire with multiple-beams – *Shine+*. Shine has multiple narrow beams, which follows *Guideline 3*, but it is designed for line-of-sight communication. Since we rely on *non-line-of-sight reflections*, we must improve Shine's reception capabilities. To achieve this goal, we implement two changes. First, we change the PD from SFH203P to SFH206K, which extend the communication range by 165%. Second, we add a low pass filter to improve the signal-to-noise ratio.

4.1.2 A medium-range luminaire with less-beams – *Shine++*. To evaluate our sensing approach with longer ranges in realistic scenarios, we build a new front-end with commercial LED bulbs, dubbed *Shine++*. We choose the IKEA Ledare LED with a viewing angle of 36 °as the

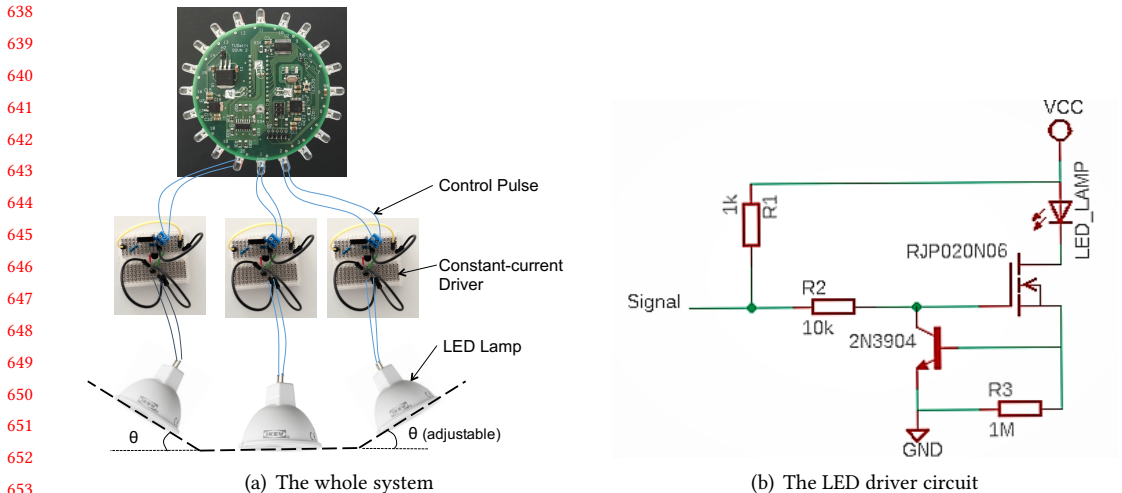


Fig. 19. Our testbed with the front-end Shine++

transmitters. We use three LED bulbs, one placed in the middle and the other two on the sides with adjustable inclination angles, as shown in Fig. 19(a). Each LED consumes 3.5 W, thus we design a new LED driver circuit to provide higher power, as presented in Fig. 19(b).

4.1.3 Software. Our software implements the data transmission and reception, the access control for the shared visible light medium, the positioning and object identification algorithms. In our application we need accurate timing to schedule the modulation of light beams. We connect all the nodes to a central server (PC/laptop), where we run a Time Division Multiple Access (TDMA) scheme. This scheme turns *on* all LEDs, but modulates only one *beam* at a time. Adaptive decoding thresholds are implemented in our system to eliminate interference from external light sources, including neighboring LEDs that are *on* but not modulated. The MAC schedules the LEDs ‘remotely’ through the interface with the micro-controllers. Similarly, the data received from the PDs are decoded at the micro-controllers and sent through the UART to the central server. Upon receiving these frames, the server runs the *positioning algorithm* (cf. Section 2.4) and calculates on-the-fly the current position of the mobile object. The outcome of the algorithm is demonstrated in a simple GUI (omitted due to the space limitation).

4.2 Object design

For passive positioning with VLC, the external surface of the objects plays a key role. Three out of the four guidelines in Section 2 pertain to the object’s surface. In this subsection we describe the surfaces we use for our evaluation and the reasoning behind selecting them.

4.2.1 A perfect reflector. As stated by our guidelines, the ideal surface would use materials with very high reflective coefficients and specular reflection to enable non-line-of-sight communication, and would consist of small reflecting areas (Guideline 1) tilted at different angles (Guideline 2) to increase coverage. We use thin strips of flat mirrors to satisfy these three guidelines. Fig. 20 presents a side view of the reflecting object, which consists of five mirrors with inclined angles of -18° , -9° , 0° , 9° , 18° , respectively. All the mirrors have the same width of 5 mm.

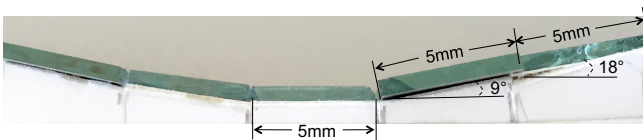
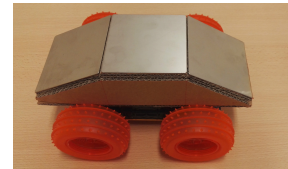
Fig. 20. Side view of the object with *perfect* reflective coefficientFig. 21. Customized toy car (*standard reflector*, 28cm×11cm×7cm)

Fig. 22. The object-ID (preamble + ID value “0”) that is attached to all the three parts of the object

4.2.2 A standard reflector. To evaluate the performance of passive positioning with more standard objects, we use a customized toy car. Such an object relaxes the requirements of our first three guidelines. The material is metal, whose reflective coefficient is not as good as mirrors. Second, the surfaces are big (relaxes Guideline 1). Third, it has few tilted angles (relaxes Guideline 2). For our object, we consider three parts of a car: the front windshield, the roof, and the back windshield. After a thorough investigation of different cars’ shapes, we decide to customize a toy car with inclined angles of -30°, 0°, 25°. The final customized car is shown in Fig. 21. Note that we are aware of the fact that different parts of a real car have different reflection coefficients, but we only use one type of material for a single toy car in this work for simplicity. We build two different toy cars, one with aluminum and the other one with mirrors.

4.2.3 Design of object-ID. We label the objects in our system with unique IDs consisting of certain patterns. The ID pattern has been presented in the Fig. 17. An object-ID consisting of the preamble and a bit “0”, is shown in Fig. 22 where it is attached to all the three faces of the customized toy car.

5 EVALUATION

In this section, we evaluate our methods under increasingly complex test cases. First we present the evaluation on positioning, followed by the evaluation on identification. Note that our passive positioning and identification methods can work at the same time, as described in Sec. 5.3.

5.1 Positioning: ideal case

For the ideal case we use the best possible setup: the front-end with many beams (Shine+) together with the perfect reflector. The experiment setup is shown in Fig. 23. We deploy two nodes (denoted as A and B) at an inter-node distance of 20 cm, and at a height of 15 cm from a desktop. **The light intensity measured at the desktop is about 450 lux under the nodes (cf. positions R2 and R10 in Fig. 24).** Shine+ can achieve reliable VLC at a distance of up to 50 cm. By deploying the two nodes as described above, we can assure that the distance travelled by the reflected signals is shorter than the maximal communication distance (i.e., 50 cm). It is also important to highlight that the angles of the perfect reflector are designed based on Propositions 1 and 2 to guarantee that every beam

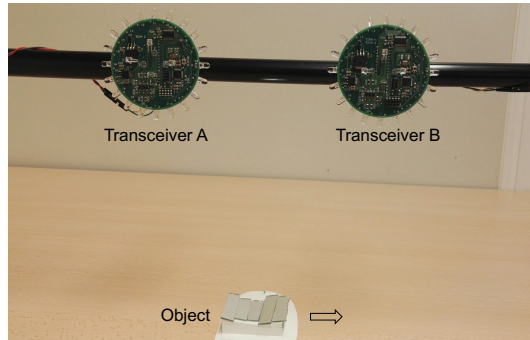


Fig. 23. Experiment setup in the ideal case (height=15 cm, inter-node distance=20 cm)

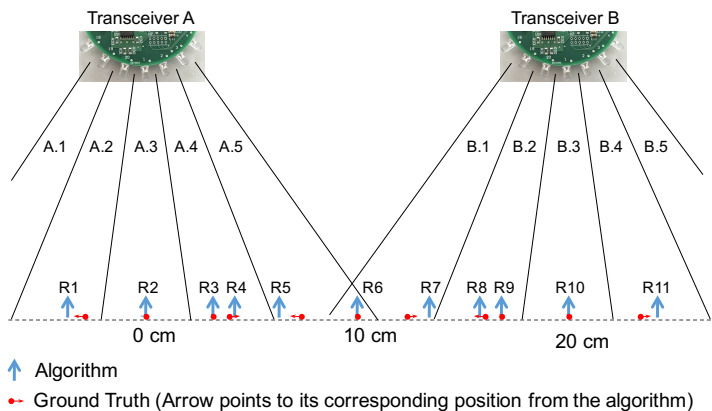


Fig. 24. Evaluation results in the ideal case

has at least one angle that will reflect the light to a neighboring node or to itself. If these angles are not selected carefully, the system may end up having beams without reflections, and thus, no positioning could be performed inside the area covered by these beams. Different inter-node distances or heights will lead to different tilted angles.

Results. The evaluation results are shown in Fig. 24. The red dots represent the ground truth. The experiments were repeated ten times and we did not observe any major variance, which is expected due to the rather deterministic propagation properties of light waves and the nearly specular reflection of mirrors. We can observe that the results from our algorithm match well the ground truth. Nearly half of the locations are localized with almost perfect accuracy, while the other locations are detected with errors up to 1.3 cm.

The detail on how these locations are detected is given in Table 6. Now let us give some more insights on how our algorithm (cf. 2.4) leads to these results. The object moves from left to right. The algorithm has all the inputs required in Step 1. The first detected point R_1 is a self reflection, i.e., transceiver A receives the reflection of beam $A.2$. The server calculates all the ground truth locations that the set of self-reflecting angles $\{\alpha_1, \dots, \alpha_k\}$ can have (Step 2). Then it calculates the valid region for this beam $A.2$ (Step 3). The algorithm detects that only one point falls in the valid region, and hence, reports that point as the estimated location. The true location is ≈ 1 cm to the right. The next two estimated locations, R_2 and R_3 , are also self-reflections. The fourth estimated location R_4 is

785 Table 2. Details of the localized positions from our algorithm in ideal case (*Number*: the detected locations; TX:
 786 transmitter; RX: receiver)

Number	R1	R2	R3	R4	R5	R6	R7	R8	R9	R10	R11
Reflection angle	-9°	0°	9°	-18°	18°	0°	-18°	18°	-9°	0°	9°
TX	A.2	A.3	A.4	A.4	A.5	A.5	B.1	B.2	B.3	B.4	
RX	A	A	A	B	B	B	A	A	B	B	B
Calculated position	-4.7	0	4.7	3.3	6.7	10	13.3	16.7	15.3	20	24.7
Measured position	-3.4	0	3.4	4.5	7.9	10	12.1	15.9	16.1	20	23.4

794 due to the communication between transceivers A and B (inter-node reflection). Notice that in this
 795 case, two locations are within the valid region of beam A.4: R3 and R4. But the fact that R3 is a self
 796 reflection while R4 is not, helps with distinguishing them. Note that R4 does not need to be under
 797 the coverage of transceiver B to achieve inter-node reflection. This is because the photodiodes used
 798 in our experiments have a wide field of view (90°). A more challenging case occurs with the next
 799 two locations (R5, R6). These two locations are within the valid region of beam A.5, and both are
 800 the result of inter-node reflection. As stated in Step 4 of our algorithm, we can either average them
 801 out at the cost of increasing the error, or exploit speed and direction information from prior data
 802 to select the most likely location. We implement a very simple mechanism to exploit direction
 803 information. Every time we detect a new point we set it as the origin, prior data are given negative
 804 values based on their distance to this last point, and new data are given positive values. If two or
 805 more positive points are estimated as locations, we select the closest one (point R5 in this case). The
 806 remainder half of the path is symmetrical to the first half, and thus, the estimation is similar to what
 807 has just been described. We don't have any location estimations for beams A.1 and B.5, because
 808 there are no self-reflecting angles for these regions. If transceiver A would have a neighbour to its
 809 left, then beam A.1 would have two potential locations (similar to R6 and R7).

811 Regarding the errors in our estimations, we found that they are due to two main reasons. First,
 812 misalignment of the angles in the moving object, e.g. our calculations in the algorithm are done
 813 assuming the tilted angles of the object are 9°, 18°, etc., while in practice there are certain errors.
 814 Second, we assume that luminaires are single-LED sources, while in practice they have multiple
 815 LEDs (5 LED sources in the case of *Shine+*). This difference changes the incidence angles, which in
 816 turn affects the estimated location. This latter point is why our errors are more pronounced at the
 817 boundaries of two beams and more accurate at the center of beams.

818 Finally, it is important to note that passive positioning with VLC operates in a fundamentally
 819 different manner compared to most positioning methods. Traditionally, after a signal is received,
 820 the positioning algorithm provides an estimated location that can be anywhere. In our method,
 821 the positioning algorithm only has a limited number of locations to choose from. The number of
 822 locations depends on the number of beams and tilted angles. Thus, upon receiving a signal, our
 823 method's task is to map the received signal to the most appropriate location, *without requiring a*
 824 *training phase*.

825 5.2 Positioning: realistic case

826 We now test our passive positioning in a more realistic case, consisting of less beams and an object
 827 with less tilted angels. In this scenario, we use two nodes equipped with the Shine++ front-end.
 828 As introduced in Sec. 4, Shine++ uses more powerful LEDs, which enable nodes to communicate
 829 at a distance of 5 m (the distance can be further by increasing the light intensity of luminaires).
 830 The experimental setup in a realistic case is shown in 25. In the tests, we set the height of the
 831 nodes to various levels: 1 m, 1.5 m, and 2 m. The height (range) can be increased if we add a lens to
 832

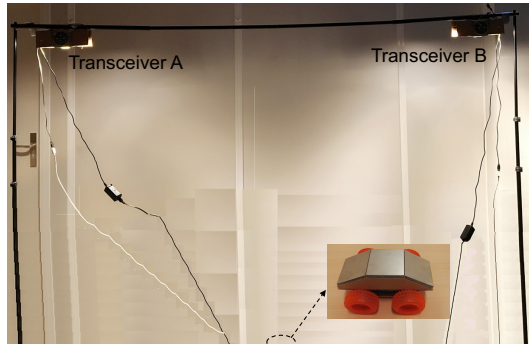


Fig. 25. Experiment setup in the realistic case

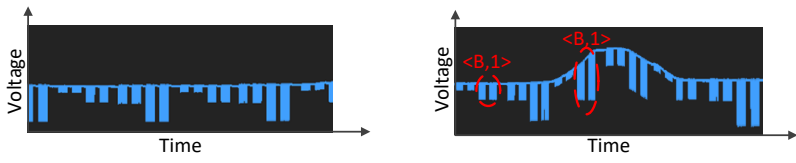
(a) PD receives beacons reflected by floor (b) PD response when object passes R_3

Fig. 26. Dealing with the floor reflection

the photodiode. Meanwhile, the inter-node distance is adjusted between 2 m and 2.5 m. The light intensity measured at the floor is about 600 lux under the nodes (cf. positions R_1 and R_5 in Fig. 27) when the height of the nodes is 1.5 m.

Dealing with floor reflection. The floor can reflect the light emitted by LEDs. When the light is modulated to send beacons, the ceiling PD can detect the transmissions of these beacons due to the floor reflection. Fig. 26(a) shows this phenomenon. When an object with a reflective surface passes under the LEDs, the PD can also detect the beacons, as illustrated in Fig. 26(b). To distinguish them in order to localize the object, we design an initialization phase in which the system sends beacons and records their depths when there is no object passing by. Then, a threshold for beacon detection is calculated based on the recorded depths. When there is a beacon depth change exceeding the threshold, e.g. the beacon $< B, 1 >$ illustrated in Fig. 26(b) (the depth of other beacons remains roughly the same), our system will know which light beam has caused the above changes and then localize the object based on this information.

Results. The evaluation results are shown in Fig. 27, where the height and inter-node distance are set to 1.5 m and 2.5 m, respectively. For this experiment we use the aluminum-car. All the six LEDs work under the *communication+illumination* mode. First, it is important to observe that in this setup we can only detect five locations, which is less than the eleven locations detected under the ideal case. This occurs because we now have less beams and less tilted angles. But all the five estimated locations are still accurate. Note that in Fig. 27, red bars are used to represent the ground-truth positions (instead of dots as in Fig. 24). This is because the surfaces are wide enough to give a continuous location range, while in Sec. 5.1 the mirrors are so narrow that only a ‘single’ point is detected. Results under different inter-node distances and heights are given

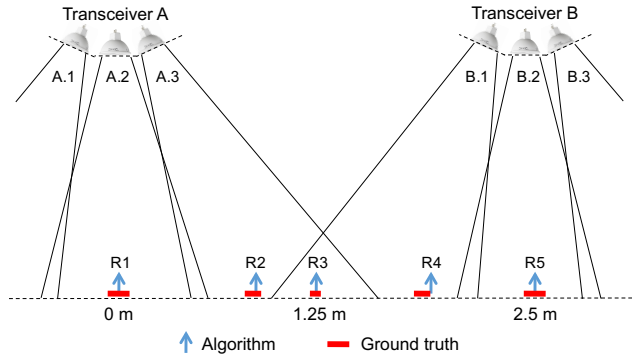


Fig. 27. Evaluation results in the realistic case (height=1.5 m, distance=2.5 m)

Table 3. Evaluation results in realistic case (height=1 m, inter-node distance=2 m)

No.	R1	R2	R3	R4	R5
Reflection angle	0°	-30°	0°	25°	0°
Algorithm	0 m	0.577 m	1 m	1.534 m	2 m
Mirror	-0.02~0.02	0.63~0.66	0.99~1.01	1.48~1.51	1.98~2.02
Aluminum	-0.02~0.02	0.62~0.65	0.99~1.01	1.47~1.5	1.98~2.02

Table 4. Evaluation results in realistic case (height=1.5 m, inter-node distance=2.5 m)

No.	R1	R2	R3	R4	R5
Reflection angle	0°	-30°	0°	25°	0°
Algorithm	0 m	0.866 m	1.25 m	1.801 m	2.5 m
Mirror	-0.02~0.02	0.85~0.88	1.25~1.26	1.76~1.78	2.48~2.52
Aluminum	-0.02~0.02	0.85~0.88	1.25~1.26	1.77~1.79	2.48~2.52

Table 5. Evaluation results in realistic case (height=2 m, inter-node distance=2.5 m)

No.	R1	R2	R3	R4	R5
Reflection angle	0°	-30°	0°	25°	0°
Algorithm	0 m	1.155 m	1.25 m	1.567 m	2.5 m
Mirror	-0.02~0.02	1.15~1.17	1.25~1.27	1.5~1.52	2.48~2.52
Aluminum	-0.02~0.02	1.13~1.15	none	1.51~1.52	2.48~2.52

in Tables 3–5. These tables show the estimations of our algorithm and the ranges of the actual locations for the aluminum- and mirror-car. From these results we can observe that the maximum positioning error is around 5.3 cm and the average error is 0.97 cm. The performances with the mirror- and aluminum-car are similar. The only difference is that in Table 5, the position R3 can be detected with the mirror-car but not with the aluminum-car (due to the lower reflective coefficient of aluminum).

5.3 Identification

We now present the evaluation on passive identification. Without loss of generality, we use the object-ID as shown in Fig. 22. In the experiment, the height of the transceivers is 1.5 m and the

inter-node distance is 2.5 m. The object is moved at a constant speed by a toy train motor from transceiver A to transceiver B. We only use the “standard reflector” in this test because the “perfect reflector” is too small to carry the object-ID.

5.3.1 Results for the scenario when LEDs operate at communication+illumination mode. The signal received by the PD of transceiver A is shown in Fig. 28(a). *We clearly observe the high-frequency signal that contains the beam-ID, which has been successfully used for positioning in our experiment (similar to Fig. 27).* Furthermore, we can observe that the object-ID appears three times: In Fig. 28(a), the corresponding signals are marked as G_1 , G_2 and G_3 . They correspond to the three positions R_1 , R_2 , and R_3 in Fig. 27, where the object is located. Note that the PD on transceiver B captures the signals of the object-ID when the object appears at the location R_3 , R_4 , and R_5 . To decode the object-ID at these positions, we first decouple signals using the downsampling based method presented in Sec. 3.1. The resulted signal is shown in Fig. 28(b), which is much cleaner. In Fig. 28(b), the first two groups of signals (G_1 and G_2) are affected by ISI. For G_1 , which is mapped to position R_1 , ISI takes effect at the tail. For G_2 (mapped to position R_2), ISI occurs at the beginning (τ is negative, cf. Sec. 3.2). For both G_1 and G_2 , we successfully used the steps presented in Sec. 3.2 to remove the ISI. The results are show in Fig. 28(c). For G_3 (mapped to position R_3), the object only modulates the light of one beam. Thus, ISI does not exist, and we can decode the object-ID directly.

5.3.2 Results for the scenario when LEDs operate at communication mode. When LEDs operate at the communication node, there is no ISI effect (cf. Section 3.2). However, we cannot directly obtain a clear envelop of the object-ID at the PD that can be used to decode the object-ID. Fig. 29 shows the signal received by the PD of transceiver A when the object passes by the position near R_1 (cf. Fig. 27). We can observe that there is no ISI effect since no envelop of the object-ID is captured by the PD. To obtain the envelop of the object-ID, we fit the envelop of the captured signals for the same beam-ID. For instance, in Fig. 29 we highlight the captured signal related to the beam $< A, 2 >$. Due to the movement of the object, the captured signal strengths are different over the time. By fitting the maximal amplitudes of these captured beam-ID signals, we can obtain the envelop of the object-ID, as shown by the red-dash line. Similarly, we can obtain the envelop of the object-ID generated due to the object’s reflection of the beam $< A, 3 >$, as denoted by the yellow-dash line. After obtaining the envelop, we can decode the object-ID, as we present in Section 5.3.1. Note that if the LEDs operate at communication+illumination mode, the two envelops mentioned above will overlap with each other in the time domain, starting from the beginning of the yellow-dash line.

6 RELATED WORK

Localization, both active and passive, has been investigated widely. In this section, we summarize the most relevant work.

Passive positioning with radio. M. Youssef *et al.* introduce the concept of Device-free Passive (DfP) positioning using Wi-Fi [Moussa and Youssef 2009; Youssef *et al.* 2007]. They show that changes in radio signals, caused by people, can be harnessed to localize a person. By comparing with the radio map that stores the signal strength in the area of interest [Youssef *et al.* 2003], the authors show that an average accuracy of 0.3 m can be achieved. Investigations in realistic environments are carried out in a follow-up work [Moussa and Youssef 2009]. Recently, researchers have also been able to track *multiple* objects passively with existing radio signals [Adib *et al.* 2015; Sabek and et al 2015]. High accuracies are achieved in these studies. We are motivated by these works to analyze the unique properties of visible light waves for *passive* positioning. Compared to radio waves, visible light waves behave in a more deterministic manner (less multipath) but have poorer coverage (because they cannot travel through opaque objects). Our study exposes the opportunities

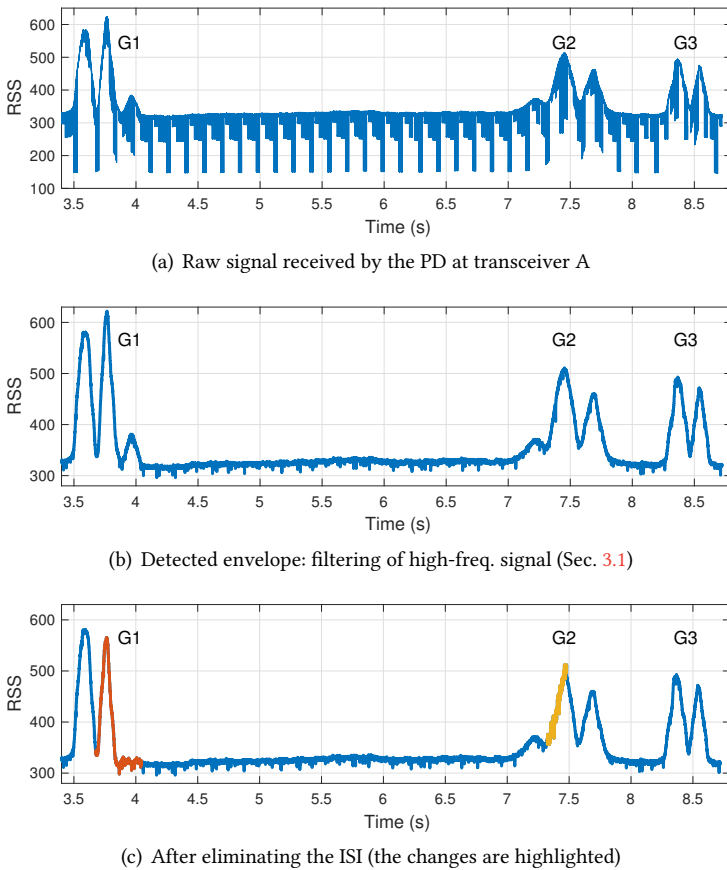


Fig. 28. Evaluation on passive identification when LEDs operate at the communication+illumination mode

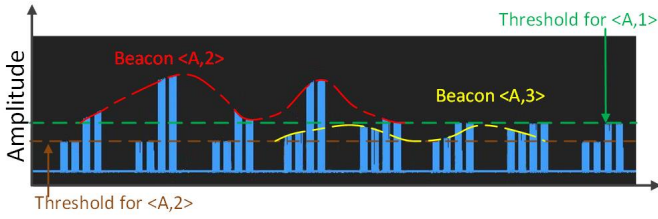


Fig. 29. Evaluation on passive identification when LEDs operate at the communication mode

and limitations of exploiting the external surfaces of objects to achieve accurate positioning and identification.

Active positioning with visible light. By leveraging the built-in camera or light sensors in smartphones, researchers have exploited *active* positioning with visible light. Epsilon [Li et al. 2014] is one of such pioneer positioning systems. In Epsilon, the smartphone is enhanced with a plugged-in photosensor to detect incident lights emitted by LED lamps. Epsilon requires at least three LED lamps as anchors such that an algorithm based on trilateration can be used to calculate the smartphone's position. It can achieve accuracies of 0.4 m to 0.8 m under different indoor environments.

This performance is improved by Luxapose [Kuo et al. 2014], which also adopts smartphone and LED luminaires as a receiver and transmitters, respectively. Unlike Epsilon, Luxapose leverages the angle-of-arrival of the signals in its positioning algorithm, and manages to achieve a better accuracy of decimeter-level. A light-weight positioning system with visible light is proposed in [Yang and et. al. 2015]. It leverages polarization-based modulation instead of intensity-based to reduce the processing workload in wearable devices. With these resource-constrained devices as receivers, it can achieve an accuracy of 3 m in 90% of the test cases. Complementary to existing work, LiPro [Xie et al. 2016] provides a solution for scenarios with insufficient reference points (LED bulbs). It tackles the case when there is only one reference point. By rotating the receiver (smartphone) around three orthogonal axes, it records continuously the RSS and magnetic field, and then calculates the receiver's position by exploiting the Lambertian radiation property [Barry 1994] of LED luminaires. LiPro can achieve a median error of 0.59 m in a corridor. In [D. Firoozabadi et al. 2019], the authors introduce a VLC method to tackle the underground localization problem. It exploits trilateration to calculate the target position. It can achieve an average error of 3.5 cm. Similar to these studies, we also rely on the Lambertian coverage of LED lights and the ideal attenuation properties of visible light waves to obtain positioning. But contrary to those studies, our method does not require carrying any photodetector with line-of-sight towards the luminaires, we exploit the reflective properties of external surfaces.

Passive sensing with visible light. Okuli [Zhang et al. 2015] was one of the work that inspired our PassiveVLP. Okuli uses an LED and two photodiodes to perform passive *near-field* sensing. It can track a finger's movement with a median error of 0.7 cm within an 8x8 cm pad. Okuli exploits the fact that fingers are round and good diffusers of light to build a model-driven solution, but it requires training data and a lighting system that is *specifically designed* for near-field positioning. Our system harnesses LEDs whose primary function is illumination and does not require any training to obtain only occupancy. Two other related studies are CeilingSee [Yang et al. 2017, 2018] and LocaLight [Di Lascio et al. 2016]. CeilingSee estimates occupancy by monitoring changes in light reflection caused by people in a room. CeilingSee uses general purpose luminaries, but they require a training phase to obtain only occupancy information. LocaLight deploys photosensors on floors to track people based on the shadows they cast. Compared to our work, the main advantage of these three systems is that they do not need to modify the external surfaces of the elements they track. We, on the other hand, modify the external surfaces, but obtain accurate positioning at longer ranges without requiring extra infrastructure (Okuli, LocaLight) or training phases (Okuli, CeilingSee).

Table 6. Summary of the most relevant work on passive localization/positioning

State of the art	Purpose	Scenario	Medium	Passive	Accuracy
[Moussa and Youssef 2009]	Localization	Indoor	Wi-Fi	Yes	0.3 m
[Adib et al. 2015]	Localization	Indoor	Radio	Yes	0.12 m
Epsilon [Li et al. 2014]	Localization	Indoor	Light	No	0.8 m
Luxapose [Kuo et al. 2014]	Localization	Indoor	Light	No	0.4 m
[Yang and et. al. 2015]	Localization	Indoor	Light	No	3 m
LiPro [Xie et al. 2016]	Localization	Indoor	Light	No	0.59 m
[D. Firoozabadi et al. 2019]	Localization	Underground	Light	No	0.0035 m
Okuli [Zhang et al. 2015]	Localization	Indoor	Light	Yes	0.007 m
CeilingSee [Yang et al. 2017]	Occupancy	Indoor	Light	Yes	-
Localight [Di Lascio et al. 2016]	Occupancy	Indoor	Light	Yes	-

Note that there is also a line of research that leverages light for secure and passive communication [Bloom et al. 2019; Wang et al. 2016; Zhang et al. 2016]. The authors in [Zhang et al. 2016] design a secure system for barcode-based VLC between smartphones. In our previous work [Wang et al. 2016], we proposed a barcode-like passive VLC system with ambient light such as sunlight. Recently, we further performed a thorough analysis on how to design a barcode to transmit information on a moving object [Bloom et al. 2019]. In all those studies, the design of barcodes with visible light is key, but those systems are designed for wireless communication. In this work, PassiveVLP, we leverage visible light barcodes not only for identification but more importantly, for localization in a passive manner.

7 LIMITATION & DISCUSSION

Many of the assumptions we make for the potential applications are realistic, such as knowing the height and geometry of luminaries. But our system also has limitations: (i) the path should not be bumpy, (ii) we can only track a few points in the paths, (iii) the system only works for 1-D scenarios, (iv) if multiple objects pass the same point simultaneously, they would cause ‘reflection collisions’, and (v) the size of the object’s surface determines the maximum number of symbols that can be encoded (maximum number of IDs), (vi) the orientation of transceivers should be stable.

Point (i) is a strong requirement, the bumpy spots in the detection area will generate outliers in our result. Our system is only resilient to few bumpy spots by eliminating outliers according to the object trace. The other five points can be improved. For point (ii), Kalman or Particle filters can be used to provide continuous location information. For point (iii), we can create annular FoVs with a single photodiode, cf. Fig. 30, to provide 2D positioning, cf. Fig. 31. Solving point (iv) with a single PD would be challenging, because it is hard to disaggregate colliding signals, a plausible alternative is to add more PDs with a narrower FoV to cover single lanes or tracks. Reducing the receivers’ FoV would also help ameliorating point (v): a narrow FoV would allow us to use narrower stripes, which would increase the number of IDs that can be encoded on the object’s surface. Some results can be found in our latest paper [Bloom et al. 2019]. To alleviate point (vi), we can store the light intensity caused by ground reflection after calibration. When there is no object passing by and the ground reflection does not match with the stored value well, we can then recalibrate the orientation of transceivers.



Fig. 30. Customized annular-FoV.

Fig. 31. 2D passive positioning.

8 CONCLUSION

In this work, we took a first step to design a passive localization system, PassiveVLP, based on visible light, where objects are not required to carry photosensors. To achieve our goal, we modify the external surfaces of objects so light reflections can provide information for localization and

identification. We define and analyze the elements of our proposed system, and implement a testbed to benchmark its performance. Our results show that visible light can provide passive identification and localization with cm-level accuracy. Passive sensing and localization with visible light is a nascent area, and thus, there is plenty of room for future work. The results from experiments confirmed the feasibility of localizing and identifying objects with visible light. While the current implementation of our system can not localize objects continuously, it succeeded to provide a subset of the objects' trajectory with high accuracy. We hope our work offers new insights in this up-and-coming domain.

ACKNOWLEDGEMENTS

We want to thank Danielle van der Werff for proposing the idea of using annular FoVs. This work was supported in part by the Social Urban Data Lab (SUDL), Amsterdam Institute for Advanced Metropolitan Solutions (AMS), the FWO postdoctoral fellowship under grant number 12Y0919N, and the FWO SBO project SAMURAI.

REFERENCES

- 802.11.bb. 2018. *IEEE 802.11 Light Communications*. Retrieved Dec, 2018 from http://www.ieee802.org/11/Reports/tgbb_update.htm
- Fadel Adib, Zachary Kabelac, and Dina Katabi. 2015. Multi-Person Localization via RF Body Reflections. In *Proceedings of the USENIX NSDI*.
- J. R. Barry. 1994. *Wireless infrared communications*. Springer.
- Rens Bloom, Marco Zuniga, Qing Wang, and Domenico Giustiniano. 2019. Tweeting with Sunlight: Encoding Data on Mobile Objects. In *Proceedings of the IEEE INFOCOM*. 1324–1332.
- G. Corbellini. 2014. Connecting networks of toys and smartphones with visible light communication. *IEEE Communications Magazine* (2014).
- Ali D. Firoozabadi, Cesar Azurdia-Meza, Ismael Soto, Fabian Seguel, Nicolas Krommenacker, Daniel Iturralde, Patrick Charpentier, and David Zabala-Blanco. 2019. A Novel Frequency Domain Visible Light Communication (VLC) Three-Dimensional Trilateration System for Localization in Underground Mining. *Applied Sciences* (2019).
- Elena Di Lascio, Ambuj Varshney, Thiem Voigt, and Carlos Perez-Penichet. 2016. Poster Abstract: LocaLight - A Battery-Free Passive Localization System Using Visible Light. In *Proceedings of IPSN*.
- L. Klaver and M. Zuniga. 2015. Shine: a Step Towards Distributed Multi-Hop Visible Light Communication. In *Proceedings of the IEEE MASS*.
- Ye-Sheng Kuo, Pat Pannuto, and et. al. 2014. Luxapose: Indoor Positioning with Mobile Phones and Visible Light. In *Proceedings of the ACM MobiCom*.
- Jiangtao Li, Angli Liu, Guobin Shen, Liqun Li, Chao Sun, and Feng Zhao. 2015. Retro-VLC: Enabling Battery-free Duplex Visible Light Communication for Mobile and IoT Applications. In *Proceedings of the ACM HotMobile*. 21–26.
- Liqun Li, Pan Hu, Chunyi Peng, Guobin Shen, and Feng Zhao. 2014. Epsilon: A Visible Light Based Positioning System. In *Proceedings of the USENIX NSDI*.
- Tianxing Li and Xia Zhou. 2018. Battery-Free Eye Tracker on Glasses. In *Proceedings of the ACM MobiCom*. 67–82.
- E. Mok and G. Retscher. 2007. Location determination using WiFi fingerprinting versus WiFi trilateration. *Journal of Location Based Services* (2007).
- M. Moussa and M. Youssef. 2009. Smart devices for smart environments: Device-free passive detection in real environments. In *Proceedings of the IEEE PerCom*.
- Philips. 2015. Philips Lighting deploys LED-based indoor positioning in Carrefour hypermarket. Retrieved Dec, 2018 from <https://goo.gl/a0tGJj>
- PureLiFi. 2012. PureLiFi. Retrieved Dec, 2018 from <http://purelifi.com>
- I. Sabek and et al. 2015. ACE: An Accurate and Efficient Multi-Entity Device-Free WLAN Localization System. *IEEE Transactions on Mobile Computing* (2015).
- Qing Wang, Marco Zuniga, and Domenico Giustiniano. 2016. Passive Communication with Ambient Light. In *Proceedings of the ACM CoNEXT*. 97–104.
- Hongjia Wu, Qing Wang, Jie Xiong, and Marco Zuniga. 2017. SmartVLC: When Smart Lighting Meets VLC. In *Proceedings of the ACM CoNEXT*. 212–223.
- Bo Xie, Shimin Gong, and Guang Tan. 2016. LiPro: light-based indoor positioning with rotating handheld devices. *Wireless Networks* (2016).

- 1177 Xieyang Xu, Yang Shen, Junrui Yang, Chenren Xu, Guobin Shen, Guojun Chen, and Yunzhe Ni. 2017. Passivevlc: Enabling
1178 practical visible light backscatter communication for battery-free iot applications. In *Proceedings of the ACM MobiCom*.
1179 180–192.
- 1180 Yanbing Yang, Jie Hao, Jun Luo, and Sinno Jialin Pan. 2017. CeilingSee: Device-free occupancy inference through lighting
1181 infrastructure based LED sensing. In *Proceedings of the IEEE PerCom*.
- 1182 Yanbing Yang, Jun Luo, Jie Hao, and Sinno Jialin Pan. 2018. Counting via LED sensing: Inferring occupancy using lighting
1183 infrastructure. *Elsevier Pervasive and Mobile Computing* (2018), 35–54.
- 1184 Zhice Yang and et. al. 2015. Wearables Can Afford: Light-weight Indoor Positioning with Visible Light. In *Proceedings of the
ACM MobiSys*.
- 1185 M. Youssef, A. Agrawala, and A. Shankar. 2003. WLAN location determination via clustering and probability distributions.
In *Proceedings of the IEEE PerCom*.
- 1186 Moustafa Youssef, Matthew Mah, and Ashok Agrawala. 2007. Challenges: Device-free Passive Localization for Wireless
1187 Environments. In *Proceedings of the ACM MobiCom*.
- 1188 B. Zhang, K. Ren, G. Xing, X. Fu, and C. Wang. 2016. SB VLC: Secure Barcode-Based Visible Light Communication for
1189 Smartphones. *IEEE Transactions on Mobile Computing* (2016), 432–446.
- 1190 Chi Zhang, Josh Tabor, Jiliang Zhang, and Xinyu Zhang. 2015. Extending Mobile Interaction Through Near-Field Visible
1191 Light Sensing. In *Proceedings of the ACM MobiCom*.
- 1192 Chi Zhang and Xinyu Zhang. 2017. Pulsar: Towards ubiquitous visible light localization. In *Proceedings of the ACM MobiCom*.
1193 208–221.
- 1194
- 1195
- 1196
- 1197
- 1198
- 1199
- 1200
- 1201
- 1202
- 1203
- 1204
- 1205
- 1206
- 1207
- 1208
- 1209
- 1210
- 1211
- 1212
- 1213
- 1214
- 1215
- 1216
- 1217
- 1218
- 1219
- 1220
- 1221
- 1222
- 1223
- 1224
- 1225